AES-Vol. 3-3

Analysis and Design of Advanced Energy Systems: Computer-Aided Analysis and Design

edited by
M. J. MORAN
R. A. BAJURA
G. TSATSARONIS

AES-Vol. 3-3

Analysis and Design of Advanced Energy Systems: Computer-Aided Analysis and Design

presented at

THE WINTER ANNUAL MEETING OF
THE AMERICAN SOCIETY OF MECHANICAL ENGINEERS
BOSTON, MASSACHUSETTS
DECEMBER 13–18, 1987

sponsored by

THE ADVANCED ENERGY SYSTEMS DIVISION, ASME

edited by

M. J. MORAN
THE OHIO STATE UNIVERSITY

R. A. BAJURA
U. S. DEPARTMENT OF ENERGY

G. TSATSARONIS
TENNESSEE TECHNOLOGICAL UNIVERSITY

THE AMERICAN SOCIETY OF MECHANICAL ENGINEERS
United Engineering Center 345 East 47th Street New York, N.Y. 10017

Library of Congress Catalog Card Number 87-73082

FOREWORD

The goal of effective energy resource utilization underlies the need for steady improvement in thermal energy systems. To this end, thermodynamic analysis is particularly relevant, especially when aided by modern optimization and computational techniques and integrated with economic considerations encountered in engineering practice. These topics provided focal points for the *Symposium on the Analysis and Design of Advanced Energy Systems* held at the 1987 ASME Winter Annual Meeting under the auspices of the System Analysis Committee of the Advanced Energy Systems Division. This volume, titled *Computer-Aided Analysis and Design* is one of three comprising papers presented at the symposium. The other two volumes are titled, respectively, *Fundamentals* and *Applications.* The division of the papers presented at the symposium into these three categroies is only approximate, for several papers might appear with equal justification under more than one of the headings.

The present symposium is but one of a series of recent or planned conferences in the general area of thermal systems analysis and design sponsored by the ASME Advanced Energy Systems Division. Readers interested in the work of a related symposium held in Rome in May 1987 should see *The Proceedings of the IV International Symposium On The Second Law Analysis of Thermal Systems,* Enrico Sciubba and Michael J. Moran co-editors (published by ASME with the identifying code I00236).

The present three volumes, together with the Proceedings of the IV International Symposium mark high water levels both for activity worldwide in thermal system analysis and design and for ASME's leadership in this field. Future symposia will build on the unprecedented activity realized in 1987, and may be expected to draw additional workers into the field while spurring the interests of those presently active.

The assistance of those individuals who reviewed articles is sincerely appreciated. In addition, the following deserve thanks for helping to chair the symposium sessions: Enrico Sciubba and William Wepfer. Finally, our greatest thanks are owed to the many individuals whose toil and technical expertise is exhibited in the papers of this volume.

Michael J. Moran
Department of Mechanical Engineering
The Ohio State University
Columbus, Ohio

Rita A. Bajura
U.S. Department of Energy
Morgantown Energy Technology Center
Morgantown, West Virginia

George Tsatsaronis
Center for Electric Power
Tennessee Technological University
Cookeville, Tennessee

CONTENTS

COMPUTER-AIDED OPTIMIZATION FOR LARGE-SIZE STEAM TURBINE POWER PLANTS: THEORY AND APPLICATION

S. S. Stecco and G. Bidini
Department of Energy Engineering
University of Florence
Florence, Italy

R. Milloni
ENEL CRTN
Pisa, Italy

ABSTRACT

A computer-aided optimization process for large-size steam-turbine plants has been developed and tested. Using the proposed numerical method, improvement of overall plant performance is achieved through optimization of extractions. A case in point is an operating 660-MW plant where improved efficiency signifies savings of approximately 1500 kW in fuel.

NOMENCLATURE

h = Enthalpy
M, $M1$, $M2$ = Flows
n = Number of extractions ($n = n' + n''$)
R = Regeneration factor
h_{sj} = Enthalpy of the steam extracted downstream of heat exchanger j ($j = 1, n$)
h_{cj} = Enthalpy of the main condensate downstream of heat exchanger j ($j = 1, n$)
h_j = Enthalpy of the steam extracted upstream of heat exchanger j ($j = 1, n$)
Wu = Specific work
η = Efficiency

Subscripts

1, 1a, 2, 2a, 3, 3a, 3b, 4, 4a = Point in the heat cycle (Figure 3)
o = Turbine inlet extraction
j = Heat exchanger index

USING COMPUTER-AIDED PROCESSES TO OPTIMIZE STEAM POWER PLANTS

While the large-size steam-turbine power plant undeniably represents a fully mature technology, research on plant optimization is still receiving considerable attention at major Western European research centers. The common objective of this intense ongoing research effort is optimization of the advanced fossile fuel plants developed in the various nations - two-shifting steam in Great Britian, combined gas-steam in Italy and West Germany, both types in Switzerland [1, 2, 3], with there being considerable room for improvement in conventional steam plants as well.

In the proposed optimization process, a numerical model utilizing special steam libraries has been devised to provide immediate calculation verification [4] and to analyze actual plant performance at contract point under specified conditions [5]. The model, herein applied at design to improve overall plant performance through extraction optimization, is applicable at both the design and operating stages. (The underlying principles of a related optimization process are detailed in [6].) It should be noted that even a tiny (i.e., one or two points per thousand) modification to stated values is significant: In fact, in a plant generating 660 MW - perhaps the most widespread size in Western Europe - one point per thousand corresponds to 660 kW!

Proper application of the process is related to three fundamental conditions:

1. Simplicity of modeling. Care should be exercised to ensure good correspondence between the modeled and actual plants.

2. Calculation speed. Speed is, of course, related to available computer power.

3. Flexibility of the model. This feature is imperative since steam plants differ considerably in terms of maximum pressures, number of heat exchangers, and pump solutions (layout, etc.).

NUMERICAL FEATURES IN SIMULATING STEAM PROPERTIES

In analyzing the exergy balance of a steam-turbine power plant, the thermophysical properties of the steam are computed with the special steam library presented in [4]. These properties may be expressed by internationally-used equations in which the T-S chart is divided into four subregions:

Region 1: Compressed and saturated liquid from 0 to 350 C delineated by the lower limit curve and the 100 MPa isobar.

Region 2: Saturated and superheated steam excluding the area around the critical point.

Region 3: Critical point and surrounding area.

Region 4: Compressed and saturated liquid from 350 °C to critical temperature.

Other equations are necessary in order to define the saturation line and the line which divides the approximately isentropic second and third regions originating on the saturation line at 350 °C. If the so-called "direct variables" (i.e., those other than temperature and pressure) are known, they can be iteratively used to determine the so-called "indirect variables" (i.e., the temperature and pressure values from which the other steam properties are derived). In the indirect variables, Regions 1 and 4 cover compressed liquids, with Regions 2 and 3 covering superheated steam. In this case, the area outside the limit curve is divided into only two regions, compressed liquids and superheated steam, by specific iterative techniques.

DESIGN CHARACTERISTICS OF THE POWER PLANT

The fundamental input design data are:

- Maximum cycle temperature and pressure.
- Superheating temperature and pressure.
- Turbomachine efficiencies.
- Deaerator pressure.
- Number of extractions present.

(Parameters of lesser importance have been omitted.)

The aim of the proposed calculation program is to perform a comparative analysis of the influence exerted on performance by varying one of the fundamental parameters within a range of significant and technically viable variations. However, certain aspects such as steam leakages, steam control labyrinths, bypass seals, etc. can be ignored at the design stage: As these do not affect selection, calculation of their effects can be left to the final verification stage once optimum conditions have been determined.

OPTIMIZING EXTRACTION PRESSURES

A typical steam plant with reheating is schematically illustrated in Figure 1; the same plant without reheating is shown simplified according to [6] in Figure 2. A description of the simplified plant's main features and how they were selected is detailed in [7], with the plant's heat cycle in Figure 3. In the simplified plant, there are 1 + M' + M" extractions mass flows, the first one at deaerator pressure P_d, with M' corresponding to low-pressure extractions and M" to high-pressure extractions. All extractions are routed to mixing surface heat exchangers.
It is commonly known that the cycle's regeneration factor may be defined as

$$R = (h_3 - h_1)/(h_2 - h_3) \qquad (1)$$

and its relative thermodynamic efficiency as

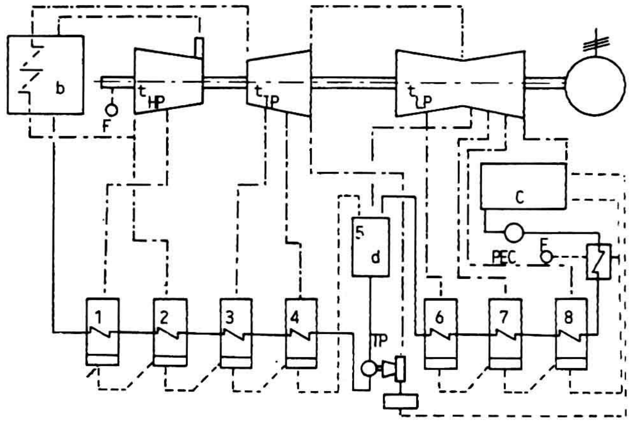

Figure 1 - A typical plant schematic

t = turbine; b = steam generator; d = deaerator; c = condenser

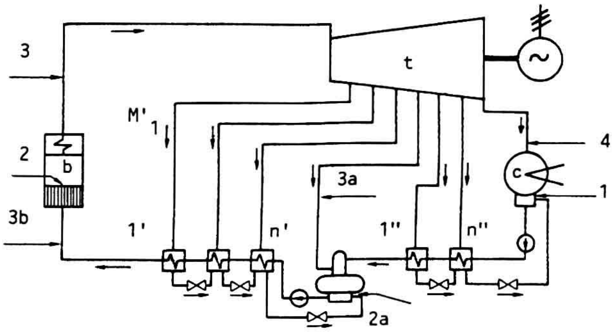

Figure 2 - Power plant without reheating

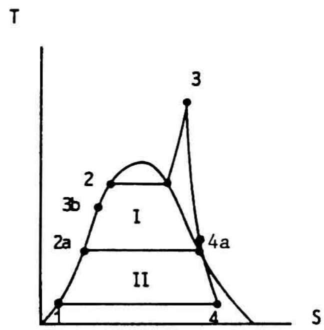

Figure 3 - Thermal cycle of plant presented in Fig 2

$$\eta = 1 - \frac{(h_4 - h_1)}{(h_3 - h_{3b})(1 + \sum_{1}^{n'} {}_jM_j' + M_o + \sum_{1}^{n''} {}_jM_j'')} \qquad (2)$$

The optimization criterion is based upon an important characteristic, i.e., that the optimum system having n extractions possesses the same efficiency as a complete regeneration plant with n + 1 extractions.

As explained in [6], the plant in Figure 1 can be modeled as in Figure 4, where the deaerator is replaced by condenser equivalent S. Note that division into a double-loop system presents notable advantages in terms of calculation time.

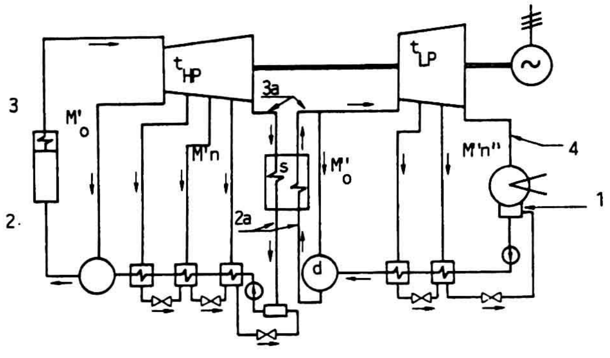

Figure 4 - Simplified schematic of "equivalent" power plant steam circuit

Efficiencies of the two cycles determined by this method can be written

$$\eta_I = 1 - \frac{(h_{4a} - h_{1a})\ M1}{(h_3 - h_2)\ M2} \tag{3}$$

$$\eta_{II} = 1 - \frac{(h_4 - h_1)}{(h_{3a} - h_{2a})\ M2} \tag{4}$$

where:

$$M1 = (1 + M_o'' + \sum_{1}^{n''} {}_jM_j'')$$

$$M2 = (1 + M_o' + \sum_{1}^{n'} {}_jM_j' + M_o'' + \sum_{1}^{n''} {}_jM_j'')$$

Observing the schematic representation of the double loop in Figure 5, it is obvious that optimization consists of rendering maximum the function

$$F = 1 + M_o + \sum_{1}^{n} {}_jM_j \tag{5}$$

Passing from Equation (5) to (6), which entails thermal balancing of the heat exchangers, the optimization process is conducted to determine the term

$$F = \frac{\left(1 + \dfrac{h_2 - h_{c1}}{h_o - h_{so}}\right)\left(1 + \dfrac{h_1 - h_{sn}}{h_n - h_{sn}}\right)}{1 + (h_{cn} - h_{sn})/(h_n - h_{sn}) - G} \tag{6}$$

where

$$G = \sum_{1}^{n-1} {}_j[(h_{c\ j} - h_{c\ j+1})/(h_j - h_{s\ j})] \prod_{j}^{n-1} {}_p[1 - (h_{s\ p} - h_{s\ p+1})/(h_{p+1} - h_{s\ p+1})] \tag{7}$$

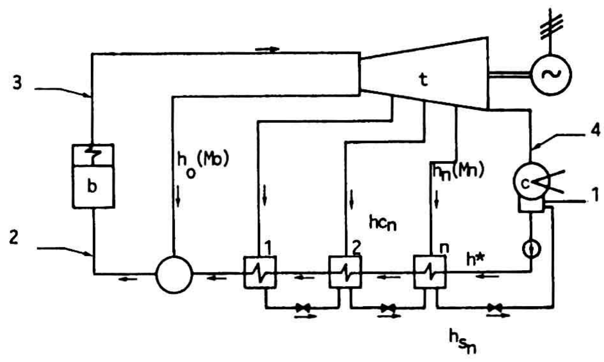

Figure 5 - Typical subsystem

Details on the numerical aspects of the solution herein omitted for the sake of brevity are given in [6].

APPLICATIONS AND FINAL COMMENTS

Verification of the model was achieved through testing of a 660-MW plant operated by ENEL, Italy's electric authority. Design plant efficiency with actual extraction pressures is, referring to the cycle and neglecting electrical generator,

$$\eta = 44.26\%$$

Proceeding according to the proposed optimization criteria yields

$$\eta = 44.36\%$$

with an increase of approximately 0.1%. For a 660-MW plant this corresponds to actual fuel savings of approximately 1500 kW.

Examination of the results reveals that the accuracy of the method for determining maximum cycle efficiency is on the order of 1 %.. This error means that optimum pressure evaluations differ in relation to the pressure-related efficiency variation - which can be considerable when the curve is flat. In the case being examined, the maximum efficiency (44.44 %) is obtained at 12 MPa for an extraction pressure at the inlet of the high-pressure heat exchanger, rather than the 15 MPa prescribed in the codes (Fig. 6).

It should be pointed out that there was significant room for improvement using the proposed model - despite the fact that we are dealing with a recently-designed and -built plant. Yet, the advantages are even greater if the optimization is implemented during the design selection stage when it is possible to weigh the consequences deriving from alternative plant solutions such as:

1. Supression or retention of an extraction(s).
2. Differences in extraction layouts.
3. Differences in pressure levels.

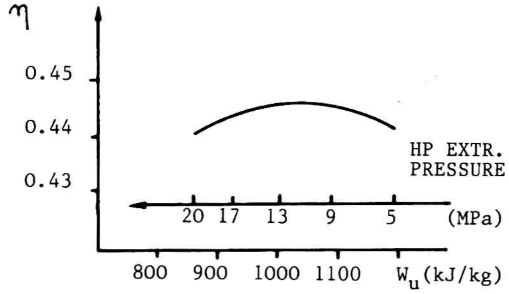

Figure 6

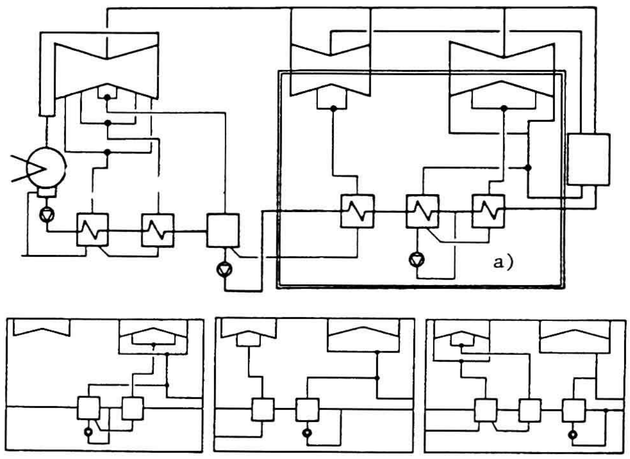

b) c) d)

Figure 7 - Schematic of various solutions.

Of these, acting on the number of extractions was felt to be the most viable approach. Hence, in the plant schematically illustrated in Figure 7, four possibilities were examined:

Condition a: Optimal reference conditions.
Condition b: Elimination of the medium-pressure extraction.
Condition c: Elimination of the first high-pressure extraction.
Condition d: Elimination of the first high-pressure extraction with doubling of the medium-pressure extraction.

The results plotted in Tables 1 and 2 speak for themselves: Elimination or repositioning of extractions have very different effects, which can be faced successfully by means of the described optimization procedure.
The proposed optimization process, applicable to a wide range of actual design conditions, provides solutions which significantly improve overall plant efficiency.

ACKNOWLEDGMENT

Contribution of MPI funding is gratefully acknowledged

REFERENCES

[1] Bertilsson, J.E. and Berg, V., " Design of Steam Turbines for Two-Shift Operations," BBC Review, April 1984.

[2] Haas, H., Engelke, W., Wald, J.E., and Termuehlen, H., "Turbines for Advanced Steam Conditions," Proceedings of American Power Conference, ASME, 1982.

[3] Wood, B., "The Question Mark over the 1300-MW Turboalternator," Steam Turbines for the 1980s, IME Conference, 1979.

[4] Stecco, S.S., Manfrida, G., and Bidini, G., "A Computer Program for Exergy Loss Modeling in Steam Turbine Power Plants," Computer-Aided Engineering of Energy Systems, ASME AES, Vol. 2.2, 1986.

[5] Stecco, S.S. and Bidini, G., "A Computer Analysis Matched To Experimental Data for Assessment of Steam Turbine Power Plant Behavior," IASTED June 29 - July 2, 1987 Lugano, Switzerland

[6] Arrighetti, C., "Un nuovo criterio per ottimizzazione nel progetto degli impianti motori a vapore regenerati," Studi e ricerche sul trattamento dei fluidi, Hoepli, Milan, Italy, 1970.

[7] Lunardi, M., "Ottimizzazione numerica della posizione degli spillamenti negli impianti a vapore," Dissertation, Florence, Italy, 1984.

[8] Stecco, S.S. and Bidini, G., "Il procedimento numerico di ottimazione degli spillamenti nelle centrali unificate," DEF-87-1 Report.

TABLE 1

EXTR. No.	COND. (Fig.7)	M FEEDRATE	h KJ/KG	p MPa	T °C
1	a	.3490	3138.	12.06	325.
	b	.3504	3138.	12.06	325.
	c	-	-	-	-
	d	-	-	-	-
2	a	.1600	2926.	3.977	250.
	b	.2703	2926.	3.977	250.
	c	.1634	2926.	3.977	250.
	d	.1329	2926.	3.977	250.
3	a	.0967	3236.	1.344	193.
	b	-	-	-	-
	c	.0981	3238.	1.350	194.
	d1	.0747	3296.	1.685	204.
	d2	.0546	3153.	.966	178.
4	a	.0807	2976.	.438	147.
	b	.0811	2976.	.438	147.
	c	.0811	2976.	.438	147.
	d	.0811	2976.	.438	147.
5	a	.0722	2762.	.140	109.
	b	.0717	2762.	.140	109.
	c	.0717	2762.	.140	109.
	d	.0717	2762.	.140	109.
6	a	.0706	2568.	.036	74.
	b	.0706	2568.	.036	74.
	c	.0706	2568.	.036	74.
	d	.0706	2568.	.036	74.

TABLE 2

CONDITIONS (Fig.7)	EFFICIENCY
a	47.67 %
b	46.39 %
c	46.41 %
d	46.65 %

COMPUTER SIMULATION WITH EXPERIMENTAL VALIDATION OF HEAT AND MASS TRANSFER IN HUMIDIFICATION PROCESSES

D. A. Kouremenos, K. A. Antonopoulos, and J. G. Koulias
Mechanical Engineering Department
National Technical University of Athens
Athens, Greece

ABSTRACT

A computer algorithm has been developed for the simulation of heat and mass transfer in humidification processes. The algorithm is based on a finite-difference solution of the momentum, heat and mass transfer differential equations and of the continuity equation, supplemented with the k-ε turbulence model in the case of turbulent flow. Experimental validation of the procedure is made in the case of a counter current annular air-water two-phase flow in a circular vertical tube. Measurements have been made of the velocity and of the dry and wet bulb temperatures in various axial and radial positions within the tube. The parameters influencing the process are numerous, including the water and air Reynolds numbers, the water film thickness, the water and air inlet temperatures, the inlet humidity of the air and the corresponding inlet velocity profile. Comparison of the experimental values with the calculated ones show that the simulation method developed in reliable.

1. INTRODUCTION

Heat and mass transfer in humidification processes is of interest in various engineering applications. This study presents a computer simulation of heat and mass transfer in the case of an air-water, annular two-phase, counter-flow within a vertical tube. As shown in Figure 1, the water flows downwards in the form of an annular thin film in the interior surface of the tube, while the air is forced upwards. The main parameters influencing this humidification process are the water and air Reynolds numbers, the water film thickness, the water and air inlet temperatures, the inlet humidity of the air and the corresponding inlet velocity profile.

The computer algorithm developed solves the momentum, energy and mass transfer differential equations together with the continuity equation by use of existing finite-difference techniques and provides the complete fields of velocity, temperature and concentration of water vapor within the air, the total pressure drop and the total evaporated mass of water. In the case of turbulent flow, the algorithm makes use of the k-ε turbulence model [1] . The choise of the two-equation k-ε turbulence model is based on the fact that zero and one-equation models require a length scale distribution to be prescribed and this is not always feasible. On the other hand, the use of higher level models requiring much more equations and computing time, whose performance is not in every case clearly established, could not be justified in the flow case examined. The use of the k-ε model implies that the more reliable predictions are to be expected at the higher Reynolds numbers.

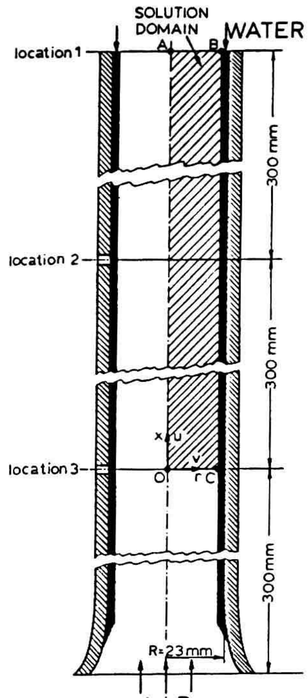

Fig.1. Test tube and solution domain. The water film flows downwards while the air is forced upwards.

For validating the algorithm developed, experiments have been performed. The measurements include the values of velocity and wet and dry bulb temperatures at various locations within the vertical tube (Fig.1), the water film thickness, the total evaporated mass of water and the total pressure drop of air flow. The measurements agree well with the corresponding calculated values.

One of the purposes for developing the present computer algorithm is to produce the data needed for constructing general correlations describing humidification processes of this kind. Such a correlation (based at present only on the measurements) which links the total evaporated mass of water to the main parameters of the humidification process, is presented.

2. EXPERIMENTS

2.1 Experimental apparatus

Measurements have been performed by employing the experimental apparatus shown schematically in Figure 2. The main part of the apparatus is the test tube 11 where the air and water film flow occurs. The tube is in vertical position, it is made from plexiglas with a wider lower end, thus facilitating the air inflow and water outflow. The internal diameter of the measurement tube is 46 mm, its lenth is 900 mm and it has apertures at appropriate locations on its surface for performing velocity and temperature measurements inside the tube. The flow of the air is developed within a 2100 mm long tube (item 7 in Figure 2), which comes before the test tube 11.

1. Variable Transformer
2. Fan
3. Air flow-meter
4. Air mixing box
5. Light
6. Inflow air thermometer
7. Entrance section
8. Adjustment system
9. Water receiving box
10. Water temperature measuring aperture
11. Test tube
12. Aperture for measuring wet bulb temperature
13. Aperture for measuring dry bulb temperature
14. Aperture for measuring velocity and pressure
15. Water inlet box
16. Water flow smoothering filters
17. Cylindrical mesh
18. Flexible air outlet duct
19. Water flow-meter
20. Thermostatic water tank and pump
21. Precision scales
22. Digital thermometer
23. Oblique tube pressure gauge and Prandtl tube
24. Piezoelectric manometer
25. Water supply regulating valve
26. Filter
27. Water regulating valve
28. Voltage stabilizer
29. Fan
30. Thermostat checking thermometer

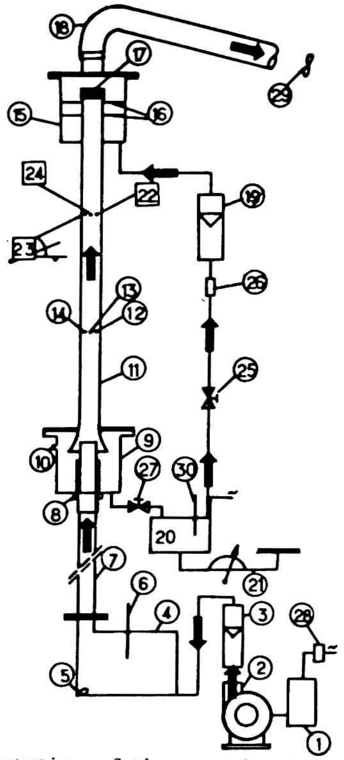

Fig.2. Schematic representation of the experimental apparatus.

2.2 Main parameters

The measurements have been performed for four different values of the three main parameters, $\dot{V}_a$, $\dot{V}_w$, t_w, defining the problem, i.e.

Air flow rate : $\dot{V}_a$ = 10.0, 15.0, 25.0, 35.0 m^3/h
Water flow rate : $\dot{V}_w$ = 54.3, 93.2, 152.8, 192.6 lt/h
Water temperature : t_w = 25.0, 30.0, 35.0, 40.0 ^oC

Therefore, the total number of cases examined is 4x4x4= =64, as shown in Table 1. The corresponding values Re_a and Re_w of the air and water Reynolds numbers are shown in the same Table.

Low water Reynolds numbers had to be employed in order to avoid formation of water ripples, as the intention here is to examine the humidification process without the uncertainty introduced in both the measurements and the numerical calculations by the formation of ripples. Low Reynolds numbers have practical applications in analogous phenomena as for example in the evaporation of NH_3 in NH_3-H_2 atmosphere employed in neutral gas absorption refrigeration units. Also, analogous situations may be found in applications concerning rectification or gas absorption columns encountered in the chemical industry.

Table 1. Cases examined and main parameters

case	$\dot{V}_w$ lt/h	$\dot{V}_a$ m^3/h	t_w ^oC	$\dot{m}_w$ gr/h	$\dot{m}_w$ from eq. (1)	error $\Delta\dot{m}_w$(%)	Re_w	Re_a
1	54.3	10	25	80.0	72.2	-9.7	115	4946
2	54.3	15	25	93.0	90.6	-2.5	115	7419
3	54.3	25	25	130.0	127.4	-1.9	115	12365
4	54.3	35	25	160.0	164.3	2.7	115	17311
5	54.3	10	30	103.5	112.1	8.3	130	4950
6	54.3	15	30	139.0	140.5	1.1	130	7425
7	54.3	25	30	206.0	197.3	-4.1	130	12376
8	54.3	35	30	260.0	254.2	-2.2	130	17326
9	54.3	10	35	156.0	160.5	2.9	142	4953
10	54.3	15	35	204.0	201.0	-1.4	142	7430
11	54.3	25	35	292.5	282.0	-3.5	142	12384
12	54.3	35	35	362.0	363.0	0.2	142	17337
13	54.3	10	40	220.0	217.5	-1.1	158	4958
14	54.3	15	40	281.5	272.1	-3.3	158	7437
15	54.3	25	40	389.0	381.5	-1.9	158	12395
16	54.3	35	40	490.0	490.8	0.1	158	17353
17	93.2	10	25	89.0	77.4	-12.9	199	4967
18	93.2	15	25	103.5	95.7	-7.4	199	7451
19	93.2	25	25	138.0	132.6	-3.8	199	12419
20	93.2	35	25	182.0	172.1	-5.4	199	17387
21	93.2	10	30	113.0	120.3	6.5	223	4972
22	93.2	15	30	142.0	148.5	4.5	223	7459
23	93.2	25	30	207.5	205.3	-1.0	223	12432
24	93.2	35	30	264.0	266.2	0.8	223	17405
25	93.2	10	35	179.0	172.3	-3.7	245	4977
26	93.2	15	35	220.0	212.4	-3.4	245	7466
27	93.2	25	35	305.0	293.5	-3.7	245	12444
28	93.2	35	35	365.0	380.2	4.1	245	17422
29	93.2	10	40	250.0	233.4	-6.6	272	4982
30	93.2	15	40	310.0	287.6	-7.2	272	7474
31	93.2	25	40	425.0	397.0	-6.5	272	12456
32	93.2	35	40	500.0	514.1	2.8	272	17439
33	152.8	10	25	94.5	85.5	-9.4	326	4992
34	152.8	15	25	112.0	103.6	-7.4	326	7488
35	152.8	25	25	150.0	140.5	-6.2	326	12480
36	152.8	35	25	212.0	184.0	-13.1	326	17472
37	152.8	10	30	120.0	132.9	10.7	366	4998
38	152.8	15	30	154.0	160.7	4.3	366	7497
39	152.8	25	30	216.0	217.6	0.7	366	12495
40	152.8	35	30	276.0	284.7	3.1	366	17439
41	152.8	10	35	183.0	190.3	4.0	402	5002
42	152.8	15	35	230.0	229.9	-0.0	402	7504
43	152.8	25	35	309.0	311.0	0.6	402	12506
44	152.8	35	35	386.0	406.6	5.3	402	17509
45	152.8	10	40	258.0	257.8	-0.0	446	5008
46	152.8	15	40	325.0	311.2	-4.2	446	7513
47	152.8	25	40	440.0	420.7	-4.3	446	12522
48	152.8	35	40	525.0	549.8	4.7	446	17531
49	192.6	10	25	98.0	91.0	-7.1	411	5004
50	192.6	15	25	117.0	108.8	-6.9	411	7506
51	192.6	25	25	162.0	145.8	-9.9	411	12511
52	192.6	35	25	214.0	192.0	-10.2	411	17515
53	192.6	10	30	128.0	141.3	10.4	462	5011
54	192.6	15	30	166.0	168.8	1.7	462	7517
55	192.6	25	30	223.0	225.8	1.2	462	12528
56	192.6	35	30	302.0	297.0	-1.6	462	17540
57	192.6	10	35	199.0	202.3	1.7	507	5016
58	192.6	15	35	247.0	241.5	-2.2	507	7525
59	192.6	25	35	336.0	322.7	-3.9	507	12541
60	192.6	35	35	400.0	424.2	6.0	507	17558
61	192.6	10	40	263.5	274.1	4.0	562	5023
62	192.6	15	40	340.5	326.9	-3.9	562	7534
63	192.6	25	40	455.5	436.5	-4.1	562	12558
64	192.6	35	40	543.0	573.7	5.6	562	17581

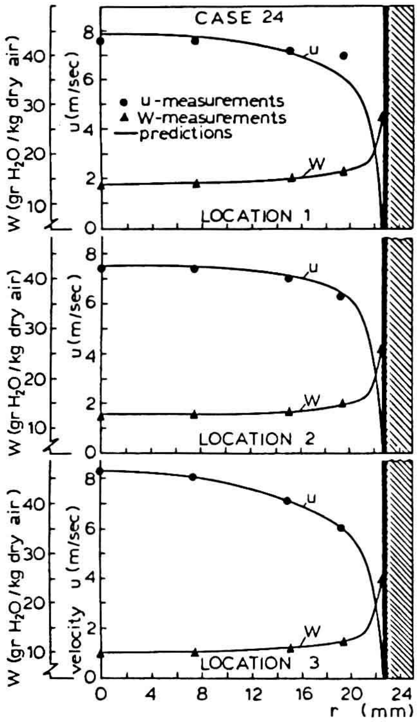

Fig.3. Measurements and numerical predictions of axial velocity and humidity ratio for case 24 ($\dot{V}_a$ = 35 m^3/h, $\dot{V}_w$ = 93.2 lt/h, t_w = 30°C).

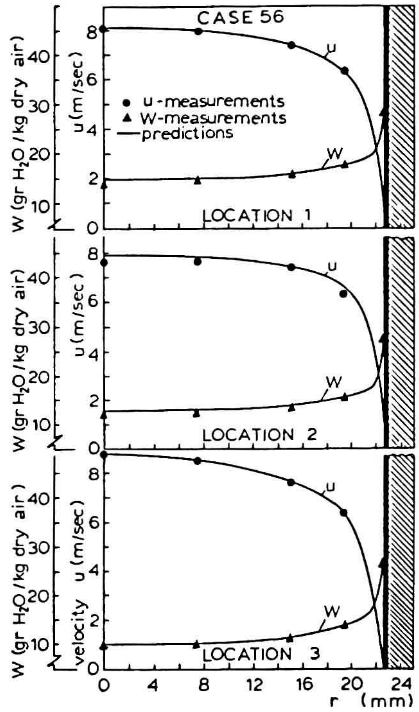

Fig.5. Measurements and numerical predictions of axial velocity and humidity ratio for case 56 ($\dot{V}_a$ = 35 m^3/h, $\dot{V}_w$ = 192.6 lt/h, t_w = 30°C).

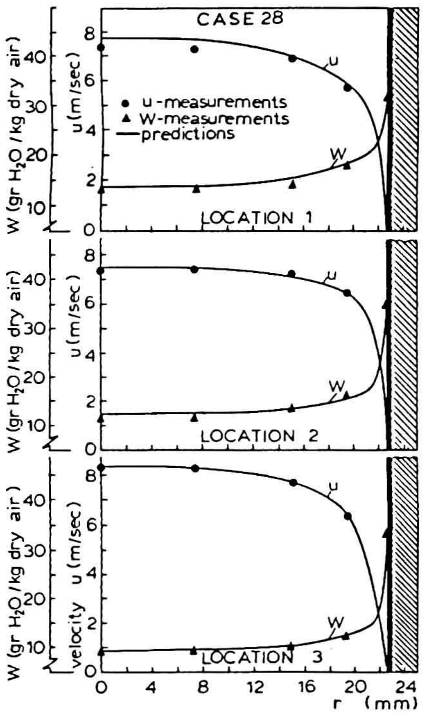

Fig.4. Measurements and numerical predictions of axial velocity and humidity ratio for case 28 ($\dot{V}_a$ = 35 m^3/h, $\dot{V}_w$ = 93.2 lt/h, t_w = 35°C).

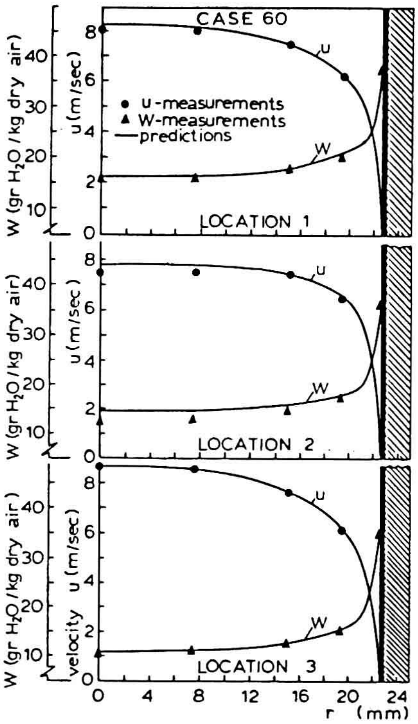

Fig.6. Measurements and numerical predictions of axial velocity and humidity ratio for case 60 ($\dot{V}_a$ = 35 m^3/h, $\dot{V}_{\ddot{W}}$ = 192.6 lt/h, t_w = 35°C).

2.3 Velocity measurements

For each one of the 64 cases of Table 1, the axial velocity u of air has been measured, by employing a 3 mm Prandtl tube, at the radial positions r = 0, r=R/3, r = 2R/3 and $r = r_{max}$ of the sections 1,2 and 3 (Figure 1). Symbol r_{max} denotes the position nearest to the water, at which measurements can be performed without the water affecting the measuring device. Examples of the measured values are shown in Figures 3 to 6, which relate to cases 24, 28, 56 and 60 respectively. In the same Figures, numerical predictions are also shown, which will be discussed later.

2.4 Temperature measurements

The local dry and wet bulb temperatures of the air have been measured by employing two thermocouples at the same positions as for the velocity. Special care has been taken for avoiding effects of conduction errors and, owing to the small temperature differences and to the surrounding cylindrical water film and tube, effects of radiation were practically absent. The thermocouple for the measurement of the dry bulb temperature was always dry because of the air flow, while the one for the measurement of the wet bulb temperature was kept wet by using a small piece of cotton continously supplied with distilled water.

The measurements have been performed for each one of the cases of Table 1. The humidity ratio W (kg water vapor/kg dry air) has been determined from the measured values of the dry and wet bulb temperatures by using the psychrometric chart. Figures 3 to 6 show examples of the humidity ratio distribution corresponding to cases 24, 28, 56 and 60.

2.5. Measurement of the evaporated mass of water

One of the most important quantities in the process examined is the total evaporated mass of water, $\dot m_w$(gr/h). This has been determined by weighing the water on its way in and out of the measurement tube, for each one of the 64 cases considered.

From the practical point of view, it is very usefull to be able to predict the final result of the humidification process, i.e. the total evaporated mass of water, $\dot m_w$, in terms of the parameters $\dot V_a$, $\dot V_w$ and t_w. For this purpose, the following correlation has been developed by least square fitting to the 64 measured values of $\dot m_w$:

$$\frac{\dot m_w}{\dot m_{wo}} = \frac{t_w}{t_{wo}}\left[-0.23-0.1953\frac{\dot V_a}{\dot V_{ao}}+(0.6719+0.656\frac{\dot V_a}{\dot V_{ao}})\frac{t_w}{t_{wo}}\right]\left[1+(\frac{\dot V_w}{\dot V_{wo}}-1)(0.056+0.016(2.7-\frac{\dot V_a}{\dot V_{ao}})^2)\right] \qquad (1)$$

where the normalizing values $\dot m_{wo}$ = 80 gr/h, $\dot V_{ao}=10m^3/h$, $\dot V_{wo}$ = 54.3 lt/h, t_{wo} = 25°C correspond to case 1. The success of the approximation is shown in Table 1, which displays the measured values of $\dot m_w$ and the calculated ones from equation (1) as well as the relative error between them.

The evaporated mass of water increases considerably with increasing air flow rate or increasing water temperature and to a much lesser extent with increasing water flow rate. Figure 7 shows the variation of $\dot m_w$ in terms of t_w with $\dot V_w$ as a parameter, in the case of $\dot V_a$ = =10m³/h, while Figures 8,9 and 10 present analogous results for $\dot V_a$ = 15, 25 and 35 m³/h respectively. All Figures show the measured values as well as the calculated ones by use of correlation (1).

2.6 Measurement of water film thickness and air total pressure drop

The mean thickness of the water film has been measured by use of an electric contact micrometer for various values of the water Reynolds number. The results are shown in Figure 11.

The total pressure drop between sections 1 and 3 (Figure 1) has been measured for each one of the 64 cases, by use of two Prandtl tubes located at the axis of the test tube.

The parameters affecting the accuracy of the measurements are numerous. Care has been taken for the uniformity of the water film thickness and for the smoothness of film free surface. The test tube was placed with precision to vertical position and the water

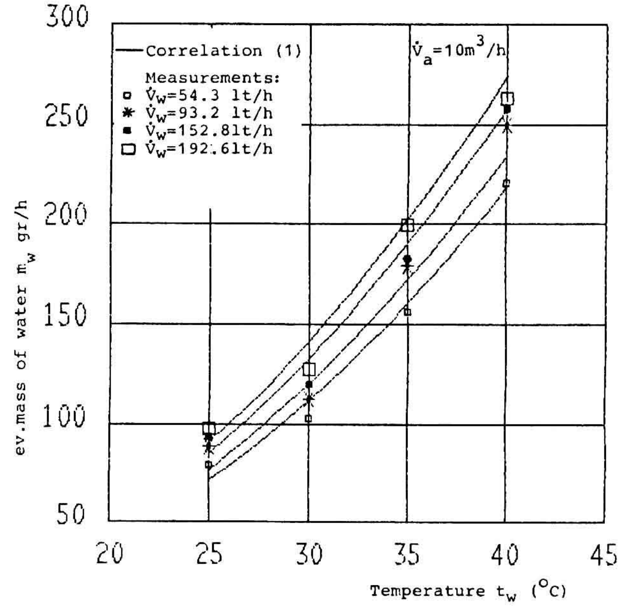

Fig.7. Total evaporated mass of water in terms of the water temperature, for air flow rate 10 m³/h.

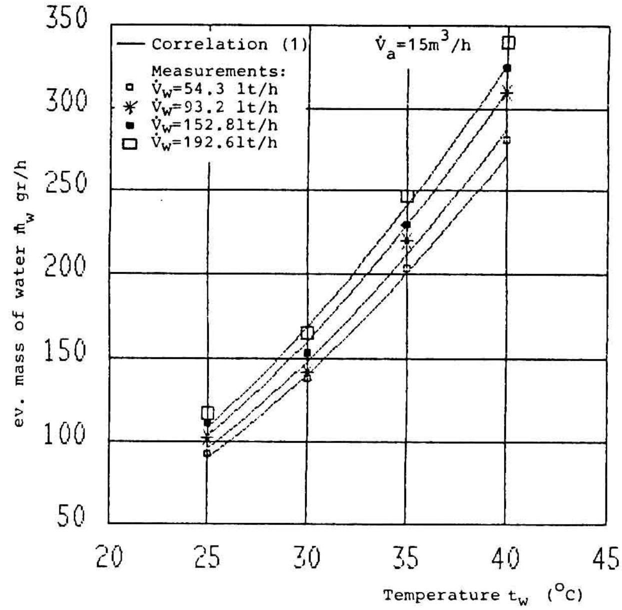

Fig.8. Total evaporated mass of water in terms of the water temperature, for air flow rate 15 m³/h.

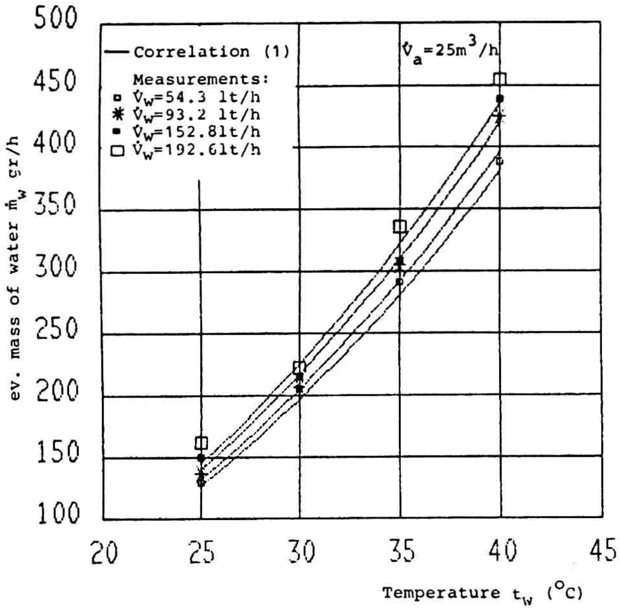

Fig.9. Total evaporated mass of water in terms of the water temperature, for air flow rate 25 m^3/h.

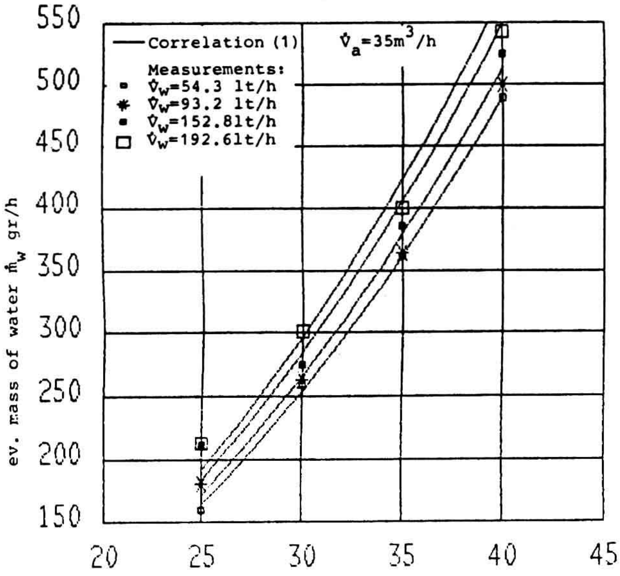

Fig.10. Total evaporated mass of water in terms of the water temperature, for air flow rate 35 m^3/h.

and air were suitably incoming into the test tube as shown in Figure 2. Also, the ambient temperature and humidity ratio were kept constant with corresponding flactuations ±0.5°C and ±0.3 gr water vapor/kg dry air. Estimation of all kinds of uncertainties introduced, suggested an error of the measurements less than 5%.

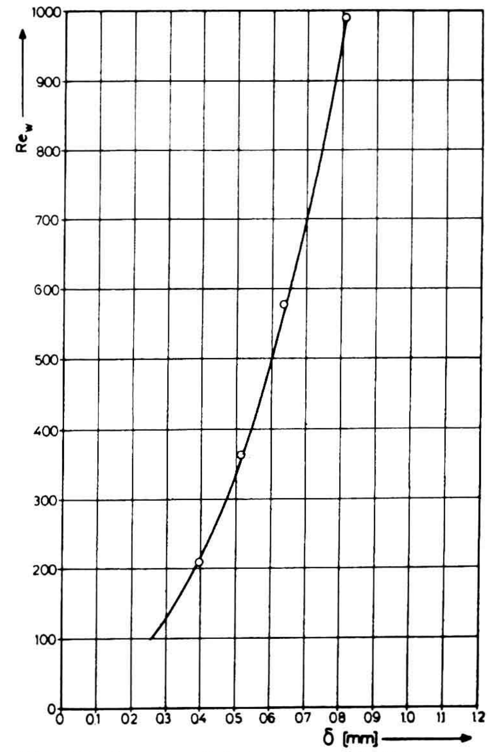

Fig.11. Measured thickness of the water film in terms of the water Reynolds number.

3.COMPUTER SIMULATION

3.1 Governing differential equations

The transport equations governing steady, two-dimensional, incompressible, viscous flow with simultaneous heat and mass transfer, may be written in terms of cylindrical polar coordinates x,r within the solution domain OABC (Figure 1) in the following common form:

$$\frac{1}{r}\left[\frac{\partial}{\partial x}(\rho u r\Phi) + \frac{\partial}{\partial y}(\rho v r\Phi) - \frac{\partial}{\partial x}\left(r\Gamma_{\Phi,eff}\frac{\partial\Phi}{\partial x}\right) - \frac{\partial}{\partial r}\left(r\Gamma_{\Phi,eff}\frac{\partial\Phi}{\partial r}\right)\right] = S_\Phi \quad (2)$$

where the general dependent variable Φ may stand for any of the following (see Table 2): the velocity component u in the axial direction x; the velocity component v in the radial direction r; the temperature T; the partial pressure of the water vapor p_w; the kinetic energy of turbulence k and the volumetric rate of dissipation of kinetic energy of turbulence ε. The quantities k and ε pertain to the turbulence model employed to simulate turbulence transport effects, details of which may be found in [1]. The terms $\Gamma_{\Phi,eff}$ and S_Φ stand for the "effective exchange coefficient" and for the "source" of property Φ, respectively, and take the values shown in Table 2. For $\Phi = 1$, $\Gamma_{\Phi,eff} = 0$ and $S_\Phi = 0$, the general transport equation (2) reduces to the continuity equation.

Symbols μ, Pr($\equiv \mu c_p/k$) and Sch ($\equiv \mu/\rho D$), appearing in Table 2, stand for the molecular viscosity, Prandtl and Schmidt numbers, respectively, while μ_t, Pr_t and Sch_t are the corresponding turbulent properties taken, according to the turbulence model employed, as

$$\mu_t = 0.09\,\rho k^2/\varepsilon \quad (3)$$

$$Pr_t = Sch_t = 1 \quad (4)$$

Quantities σ_k and σ_ε are turbulent Prandtl numbers for the transport of k and ε and are taken equal to 1 and 1.22 respectively. The expression for the term G, which stands for the generation of turbulence kinetic energy, may be found in [2]. Lastly, the symbol p, in the table, denotes the local pressure.

Table 2. Values of the variable Φ and of the terms $\Gamma_{\Phi,eff}$ and S_Φ contained in the general transport equation (2).

Transport equation	Φ	$\Gamma_{\Phi,eff}$	S_Φ
x-momentum	u	$\mu+\mu_t$	$-\frac{\partial p}{\partial x}$
r-momentum	v	$\mu+\mu_t$	$(\mu+\mu_t)\frac{v}{r^2} - \frac{\partial p}{\partial r}$
energy	T	$\frac{\mu}{Pr} + \frac{\mu_t}{Pr_t}$	0
mass	p_w	$\frac{\mu}{Sch} + \frac{\mu_t}{Sch_t}$	0
turbulence kinetic energy	k	$\frac{\mu+\mu_t}{\sigma_k}$	$G-\rho\varepsilon$
dissipation of turbulence kinetic energy	ε	$\frac{\mu+\mu_t}{\sigma_\varepsilon}$	$1.44G\frac{\varepsilon}{k} - 1.92\rho\frac{\varepsilon^2}{k}$
continuity	1	0	0

3.2 Properties of the wet air

The molecular viscosity μ of the wet air is calculated with good accuracy for T < 310 K, from the dry air relation [3]:

$$\mu = 145.8\times10^{-8}\frac{T^{3/2}}{T+110.4} \quad (kg/m\ sec) \tag{5}$$

In the pressure and temperature ranges considered, the density ρ of the wet air can be evaluated from the ideal gas relation [4]:

$$\rho = \frac{1+W}{R_a+WR_w}\frac{p}{T} \tag{6}$$

where R_a(= 287 J/kg K) and R_w(= 462 J/kg K) are the constants of the air and of the water vapor, respectively. The humidity ratio W is linked to the partial pressure of water vapor, p_w, via relation [4]:

$$W = 0.62198\frac{p_w}{p-p_w} \tag{7}$$

The molecular diffusion coefficient D of the water vapor in solution in the air is calculated from relation [5]:

$$D = 2.305\times10^{-5}\frac{1.0133}{p}\left(\frac{T}{273}\right)^{1.81} \quad (m^2/sec) \tag{8}$$

where p in bar and T in K.

3.3 Boundary treatment and solution procedure

In the present simulation, equation (2) for Φ = u,v,T,p_w,k,ε, 1 is solved by a finite-difference procedure outlined later, within domain OABC (Figure 1). The interface between the wet air and the water film (boundary CB) is treated as a wall moving downwards with velocity equal to the mean velocity of the water. The radial velocity v is taken equal to zero on this boundary, while the temperature, T, and the partial pressure of water vapor, p_w, along the tube are prescribed analytically as:

$$(T)_{CB} = a_t x^2+b_t x+c_t \tag{9}$$

$$(p_w)_{CB} = a_p x^2+b_p x+c_p \tag{10}$$

where the coefficients a,b,c have been calculated by least square fitting of the above 2nd order polynomials to the saturation T and p_w values on the film surface at locations 1,2 and 3 (Figure 1), which are known from the experiments. For imposing the boundary conditions for u,v,T,p_w and the ones for k and ε along the "wall" boundary CB, the "Wall Function" treatment has been adopted details of which may be found in [2].

Analytical functions describing the variations of u,T and p_w in terms of the radial coordinate r, have been employed along the inlet boundary OC. These functions have been derived by curve fitting to the available measurements along boundary OC. The radial velocity on boundary OC has been taken $v\simeq0$ and the distributions of k and ε are approximately those corresponding to fully-developed turbulent flow (of appropriate turbulence level) in a straight duct of circular cross-section.

At outflow boundary AB only the distribution of the normal velocity u has to be specified. It is calculated during the numerical solution procedure by adding to the adjacent interior nodal values an increment such that the overall continuity is maintained.

Lastly, on the symmetry axis OA, the velocity component normal to the axis is zero as are the normal gradients of all other variables.

The methodology of the TEACH series of computer programs [6] has been employed for solving differential equation (2) for Φ = u,v,T,p_w,k,ε,1. A computational grid of coordinate lines is generated within the solution domain and the differential equations are integrated over the control volumes of this grid to yield finite-difference equations of the form:

$$A_p\Phi_p = \sum_n A_n\Phi_n+S \tag{11}$$

$$n = N,S,E,W$$

where the coefficients A express the combined effects of convection and diffusion as described in [7]. The summation is over the neighbours N,S,E,W of the typical node P of the grid. The solution of the resulting difference equations is performed by use of the SIMPLE algorithm [8].

3.4 Results

The computer simulation outlined above has been tested succesfully in the cases of Table 1 for isothermal flow, i.e. equation (2) for Φ = T has not been solved, for the reasons explained below:

The properties affected by the temperature (which in extreme cases varies from T_{air} = 25°C to T_{water} = 40°C) are the molecular viscosity μ and the molecular diffusion coefficient D, according to equations (5) and (8) respectively, and the density ρ of the wet air, according to equation (6). Because of the turbulence, the "effective" viscosity and the "effective" diffusion coefficient are much greater than the corresponding molecular values and therefore the influence of the temperature becomes negligible. The temperature, in the extreme case of T_{air} = 25°C, T_{water} = 40°C, causes a 5% increase of the air density only very near the water film. As shown by the present predictions, this increase causes only 1% maximum change in the velocity and humidity fields, because most part of the air is retained to 25°C-27°C apart from a thin layer near the water where the temperature reaches 40°C. Because of the small influence of the temperature (i.e. less than 1%),